Journal of Experimental Nanoscience
Publication details, including instructions for authors and subscription information:
http://www.informaworld.com/smpp/title~content=t716100757

Foam-derived multiferroic $BiFeO_3$ nanoparticles and integration into transparent polymer nanocomposites

Sebastian Wohlrab[a]; Hongchu Du[a]; Margarita Weiss[b]; Stefan Kaskel[a]
[a] Department of Inorganic Chemistry, Technical University of Dresden, Dresden, Germany [b] Institute of Structure Physics, Triebenberg Laboratory, Technical University of Dresden, Dresden, Germany

To cite this Article Wohlrab, Sebastian , Du, Hongchu , Weiss, Margarita and Kaskel, Stefan(2008) 'Foam-derived multiferroic $BiFeO_3$ nanoparticles and integration into transparent polymer nanocomposites', Journal of Experimental Nanoscience, 3: 1, 1 — 15
To link to this Article: DOI: 10.1080/17458080801935597
URL: http://dx.doi.org/10.1080/17458080801935597

Journal of Experimental Nanoscience
Vol. 3, No. 1, March 2008, 1–15

Taylor & Francis
Taylor & Francis Group

Foam-derived multiferroic $BiFeO_3$ nanoparticles and integration into transparent polymer nanocomposites

Sebastian Wohlrab[a], Hongchu Du[a], Margarita Weiss[b] and Stefan Kaskel[a]*

[a]*Department of Inorganic Chemistry, Technical University of Dresden, Dresden, Germany;*
[b]*Institute of Structure Physics, Triebenberg Laboratory, Technical University of Dresden, Dresden, Germany*

(*Received 5 January 2007; final version received 22 January 2008*)

Transparent $BiFeO_3$/PMMA (PMMA = poly(methyl methacrylate)) nanocomposites with a thickness up to 40 μm are obtained via solution film casting of $BiFeO_3$ nanoparticle dispersions. The multiferroic $BiFeO_3$ nanoparticles are obtained in a space confined crystallisation process in a porous carbon matrix and subsequent removal of the matrix. The average crystallite size ranges from 46 nm to 106 nm for materials synthesised at 803 K and 903 K respectively, but, at higher temperature, significant amounts of side products are detected by means of X-ray powder diffraction. The nanoparticles are multiferroic with a magnetic coercivity of 1.88 $A\,m^{-1}$ at 400 K and a polarisation of up to 1.04 $\mu C/cm^2$ at 65 kV/cm (298 K). Surface functionalisation using oleic acid allows the integration into PMMA films with a high transmittance.

Keywords: $BiFeO_3$; multiferroic; nanoparticles; nanocomposite

1. Introduction

Currently, there is a strong interest in multiferroic materials, due to potential applications in magnetic and ferroelectric devices, spintronics, or sensors. Coupling of ferroelectric and ferromagnetic properties can be achieved in composites by combining two different types of inorganic materials or by the integration of magnetic particles inside a ferroelectric polymer. An early example consisted of a piezoelectric phase $BaTiO_3$ and a ferromagnetic phase $CoFe_2O_4$ [1], and in recent years numerous examples were realised using the composite approach [2–7]. In contrast to materials designed by combination of two different phases, a limited number of compounds are known with ferroelectric and (anti)ferromagnetic properties in a single phase [8]. Examples of such compounds with strong magnetoelectric coupling are $RMnO_3$ (R = Ho, Tb) [9,10], RMn_2O_5 (R = Gd, Eu) [11] as well as $BiFeO_3$ [12], $BiMnO_3$ [13], and $CdCr_2S_4$ [14,15].

Compounds with intrinsic multiferroic behaviour allow for the integration of two different functions in a single compound and are thus valuable components for the functionalisation of polymers. Our interest is the development of nanoparticles for the

*Corresponding author. Email: Stefan.Kaskel@chemie.tu-dresden.de

ISSN 1745–8080 print/ISSN 1745–8099 online

DOI: 10.1080/17458080801935597
http://www.informaworld.com

functionalisation of transparent polymers [16–18]. In Raleigh theory, the intensity of the scattered light is proportional to d^6 (d = particle diameter) and thus small particles and narrow particle size distributions are necessary to obtain highly transparent composites. A crucial step for the integration in polymers is surface functionalisation, since particles less than 100 nm in diameter tend to agglomerate inside polymer matrices and agglomeration leads to the formation of turbid composites.

The size effects of ferroic nanoparticles are of fundamental interest. Ferromagnetic nanoparticles become superparamagnetic below a critical particle diameter, whereas ferroelectric particles lose the ferroic properties below a critical diameter. The temperature dependence of the Curie temperature of ferroelectric particles has been described using a crystal-liquid transition model in which D_0 describes a critical particle size where the ferroelectric phase cannot exist. D_0 was estimated to be 110 nm for $BaTiO_3$ and 11.8 nm for $PbTiO_3$ nanoparticles [19]. Thus, for the integration of ferroic properties into transparent polymers, the challenge is to synthesise crystalline particles in a certain medium size range in which the ferroic properties are still observed but light scattering is minimised due to the small particle diameter. For multiferroic nanoparticles, the size-dependence of the magnetoelectric coupling is also of fundamental interest.

The multiferroic $BiFeO_3$ is ferroelectric with a high Curie temperature of 1103 K, and weak ferromagnetic properties below the Neel temperature of 643 K. For one-dimensional $BiFeO_3$ nanomaterials such as thin films, several manufacturing methods are known. $BiFeO_3$ in a thickness range of 50 to 500 nm shows a high polarisation of 50–60 $\mu C/cm^2$ as compared to bulk materials (6.1 $\mu C/cm^2$) [12]. The preparation of $BiFeO_3$ nanotubes was described using the infiltration of anodic alumina templates with 200 and 100 nm pore size [20], and nanoparticles were obtained using sol-gel methods [21]. The citric acid method was used for the preparation of $BiFeO_3$ particles 3 to 16 nm in diameter [22].

Ferromagnetic nanoparticles of various metals [23], Fe [24], Co [25,26], Fe/Fe-oxide [27] or Fe_3O_4 [28,29], were already incorporated within polymeric matrices. Materials such as $Bi_3Ti_4O_{12}$ [30,31,32], $Pb(Zr_{0.52}Ti_{0.48})O_3$ (PZT) [33,34], $PbTiO_3$ [35,36], (PB, Sr)TiO_3 [37] and $BaTiO_3$ [38,39] have been embedded into several different polymers in order to integrate new properties into conventional transparent polymers. To our knowledge, as yet, single phase multiferroic materials have not been incorporated into transparent polymers. In the following, we present the integration of single phase multiferroic $BiFeO_3$ nanoparticles into PMMA films without agglomeration. The nanocomposites have a high transmittance due to the small particle diameter.

2. Experimental section

2.1. *Chemicals*

The inorganic salts $Bi(NO_3)_3$ and $Fe(NO_3)_3$ (>99%, Gruessing), polyvinylalcohol (PVA, purity >98%, Merck, $M_r = 120000$ g/mol), polymethyl methacrylate (PMMA, Plexiglas® 7N, Degussa), tetrahydrofuran (THF) (99,9%, Acros), oleic acid (vegetable, extra pure, Merck), polyvinylcarbazole (PVK, Aldrich, M_w 1.100.000 g/mol), *n*-pentane (>99%, Fluka), ethanol (>99,8%, Fluka), and D-sucrose (>98%, Fluka) were used without further purification.

2.2. *Syntheses*

The experimental steps of the synthesis are shown in Scheme 1.

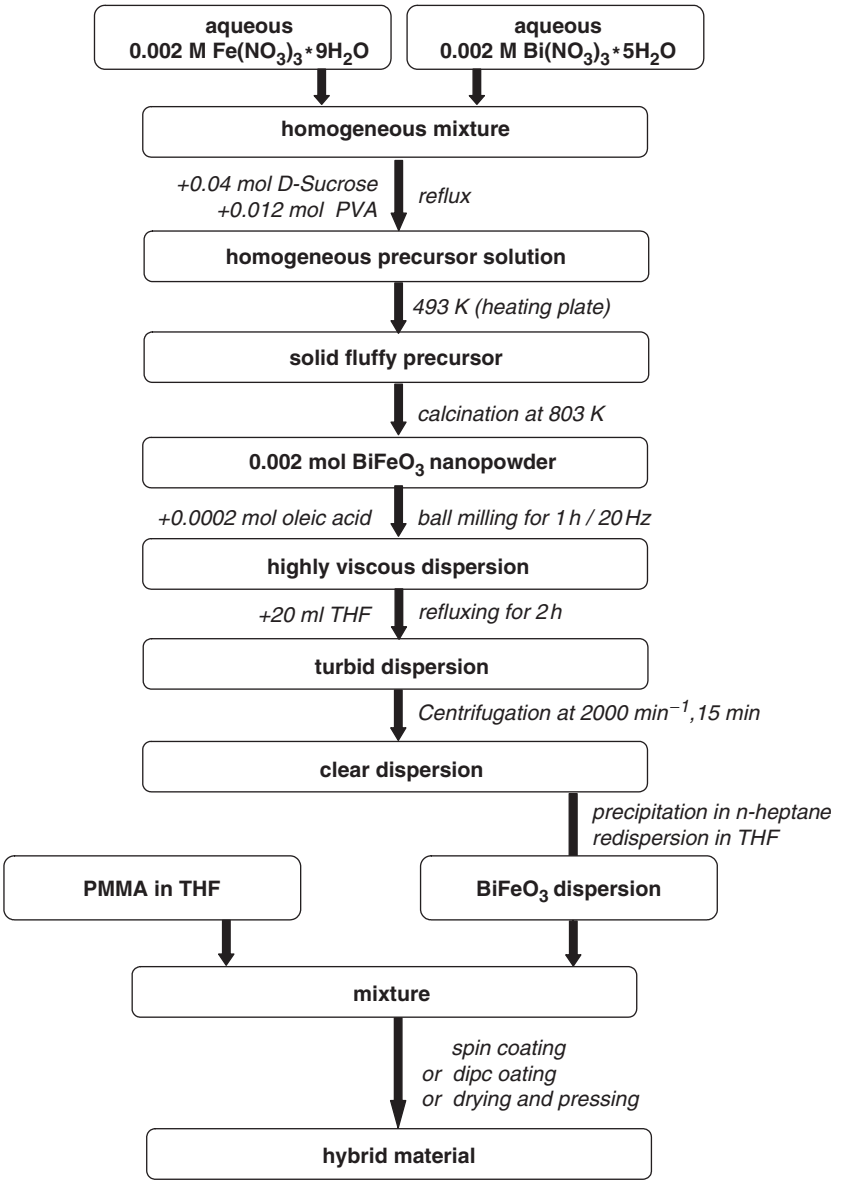

Scheme 1. Synthesis of $BiFeO_3$ nanoparticles for the integration into transparent polymers.

$Bi(NO_3)_3$ and $Fe(NO_3)_3$ were mixed together in a 1 : 1 molar ratio. After dissolution of 1 g of the mixture in 20 ml bidistilled water, 32 g of a mixture of PVA and D-sucrose in a mass ratio of 1:10 was added. After heating to 363 K for 1 h, all solid material was dissolved. The resulting solution was evaporated to a water content of 20% of the starting value. From this highly viscous mixture, the precursor was produced by heating for 30 min at 493 K. After foam thermolysis at 803 K to 1153 K, performed for the different thermolysis steps BF1-BF7 in 50 K steps, a brown powder was obtained. Herefore, the samples BF1 to BF7

were placed in a preheated oven for 30 min each. After the reaction time, the samples were removed from the oven to cool them rapidly to room temperature.

Ball-milling with 50 rel.% of oleic acid (related to the mass of the powder BF1) for 1 h at 30 Hz with a Retzsch ball-mill resulted in a brown mixture. Subsequently, THF was added to give a 1.0 wt.% $BiFeO_3$ dispersion. After ultrasonification for 180 min, larger particles were separated by centrifugation at 2000 min^{-1} for 15 min, to give a 0.25 wt.% $BiFeO_3$ dispersion (fraction 1). The dispersion was destabilised by adding *n*-pentane for coagulation of the particles. The coagulated $BiFeO_3$ was washed three times with n-pentane and subsequently peptised in THF with the help of ultrasonification. The fraction 2 was prepared from the fraction 1 by separating larger particles via centrifugation at 6000 min^{-1} for 15 min.

The nanocomposites were prepared on glass slides (76 × 26 mm) by mixing 1 ml of the BF1 dispersion (fraction 1) with different amounts of a 10% solution of PMMA and 1.0% solution of PVK in THF using spin coating (3000 min^{-1}). Before use, the slides were cleaned using ultrasonification treatment for 5 min in acetone. The thickness of these films was estimated with the help of the coated solid content and film area, to be around 1 μm.

Dip coating on a glass substrate was performed using the above mentioned mixtures in different ratios. The dip coating was performed by dipping the glass slide by hand into the polymer/particle solution. After this procedure the glass slide was dried in the perpendicular orientation at 333 K in a drier for 2 h. Taking the amount of dip coated solid and the area of the film into account, the film thickness was estimated to be around 1 μm.

Forty μm thick samples were prepared by drying the above mentioned liquid mixtures. They can be varied with the nanoparticle to polymer ratio, containing the $BiFeO_3$ particles from fraction 1 and the PMMA or the PVK solution. Pressing between indium tin oxide (ITO) coated glass slides at 403 K for 1 h yielded the PMMA composite and 503 K for 10 min the PVK composite. Three composites with different $BiFeO_3$ concentrations (2.6, 5.4 and 7.6 wt.%) were prepared using this technique.

2.3. *Techniques*

The temperature treatment was carried out in a calcination oven using a N7/H (Nabertherm). Ball-milling was performed on a Retzsch mixer mill MM200 at 20 Hz for 30 min. Ultrasonic treatment was carried out on an ultrasonic agitator, Bandelin electronic, RK 103H. Centrifugation was carried out in a centrifuge by Hein Janetzk KG, Engelsdorf Leipzig, type T23 at 2000 respectively 6000 min^{-1}. Powder X-ray diffraction patterns were recorded in transmission geometry using a STOE Stadi-P diffractometer and $CuK_{\alpha 1}$ radiation ($\lambda = 0.15405$ nm). The average crystallite size was calculated from the Scherrer equation (full pattern STOE Size/Strain analysis) with an estimated error of 5–10%. The nitrogen physisorption isotherms were measured at 77 K using a Quantachrome Autosorb 1C apparatus. Specific surface areas were calculated using the BET equation (according to Brunauer, Emmett and Teller) [40] in a relative pressure range between $P/P_o = 0.05$–0.2 (P/P_o = partial pressure) with an estimated error of 5–10%. For scanning electron microscopy (SEM), a Zeiss DMS 982 Gemini field emission microscope equipped with Noran Voyager energy-dispersive X-ray spectroscope (EDXS) was used. The as received samples were placed on a SEM sample holder and

sputtered with Pd. To fit the films to the sample holder, the substrate was cut into 5×5 mm pieces without destroying the covering film. Dynamic light scattering was performed on a Zetasizer Nano-ZS from Malvern Instruments at 298 K assuming spherical particle shape. Ferroelectric measurements were carried out using a Radiant Ferrotester combined with a high voltage amplifier from TREK, Inc. (610 E). Tablets of the $BiFeO_3$ powders BF1 and BF6 with 200 μm in thickness were pressed and sputtered with Pd. Measurements from 0 to 1500 V were carried out with the help of this system in order to get information of hysteresis behaviour. At each applied voltage, first conductivity was tested to ensure isolating behaviour of the sample. The nanocomposite film was prepared from a mixture of the 10% PMMA in THF and the $BiFeO_3$ dispersion mentioned above (BF1, fraction 1) by drying and pressing between two glasses at 403 K using a Teflon spacer (40 μm thickness) between the electrodes. The magnetisation of the as received powders was measured in a SQUID (Superconducting quantum interference device) magnetometer (MPMS XL–7, Quantum Design) at temperatures in between 2 K and 400 K. The transmission electron microscopy (TEM) images were taken with a Phillips CM200FEG system with integrated Lorentz lens. UV/Vis-measurements were carried out on a Shimadzu UV1650PC machine using the 40 μm thick composite films without the glass. Spin coating was carried out using a spin coater, SPIN 150, from S.P.S. Vertriebs GmbH. Thermogravimetric analysis was performed on a Netzsch STA 409 system in the range from 293 to 1173 K at 10 K/min.

3. Results and discussion

3.1. *Synthesis of $BiFeO_3$ nanoparticles within an exo-template*

A key problem for the integration of complex oxides into polymers is the high crystallisation temperature of many ferroelectric oxides. Ternary oxide nanoparticles synthesised in solution can be well defined in terms of size, but are often X-ray amorphous. However, crystallisation at higher temperatures is associated with diffusive mass transport, and thus the sintering step causes uncontrollable aggregation and crystal growth. One way to avoid this problem is to perform the crystallisation inside a protecting matrix. Subsequent removal of the matrix results in isolated particles and thus sintering and crystal growth is minimised and suppressed. Recently, we have developed a foam-assisted method for the preparation of catalytic vanadium nitride (VN) nanoparticles [41]. In the following, we describe a foam-assisted method for the preparation of nanosized multiferroic $BiFeO_3$ nanoparticles producing particles suited for the integration in polymer materials.

For this purpose a sucrose/PVA-matrix can be used for embedding bismuth and iron precursors. In the course of the foam thermolysis at temperatures between 803 K and 1103 K the matrix decomposes, leaving inorganic matter as nanoscale product. The products obtained at different temperatures are listed in Table 1.

Based on X-ray powder diffraction patterns (Figure 1), $BiFeO_3$ (Powder diffraction file – PDF: 20–169, from International Centre of Diffraction Data (ICDD)) is obtained at 803 K to 1053. At higher temperature, $BiFeO_3$ decomposes and the peaks are in good agreement with those of $Bi_{36}Fe_2O_{57}$ (PDF: 42–181) or $Bi_{24}Fe_2O_{39}$ (PDF: 42–201). The most intensive reflections of these bismuth-rich phases are also present as an impurity in BF5 and BF6. The formation of Bi-rich phases in the preparation of $BiFeO_3$ has been reported earlier [42].

Table 1. Synthesis conditions and properties of the $BiFeO_3$ particles synthesised via the foam method.

Sample	$T_{synth.}$ [K]	Phase composition	d [nm][a]	d_S [nm][b]	S_g [m^2/g][c]
BF1	803	$BiFeO_3$	46	12	61
BF2	853	$BiFeO_3$	77	20	36
BF3	903	$BiFeO_3$	106	80	9
BF4	953	$BiFeO_3 + A^d$	–	120	6
BF5	1003	$BiFeO_3 + A^d$	–	–	–
BF6	1053	$BiFeO_3 + A^d$	–	–	–
BF7	1103	A^d	–	–	–

[a]Crystallite diameter d from Scherrer equation, [b]calculated from $S_g = 6/\rho d$ (ρ-density), [c]specific BET surface area, [d]A: Bi-rich side product ($Bi_{36}Fe_2O_{57}$ or $Bi_{24}Fe_2O_{39}$).

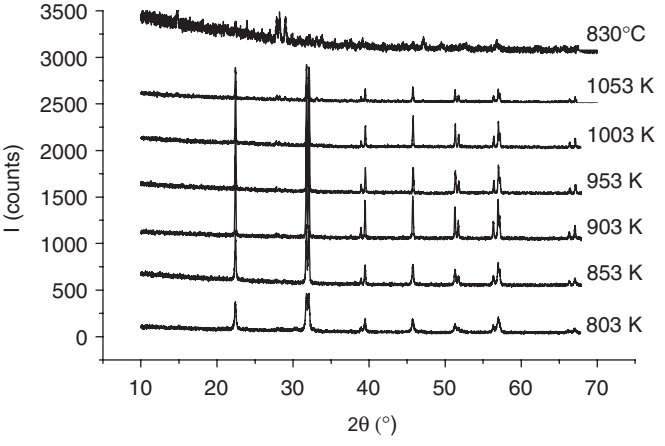

Figure 1. X-ray powder diffraction patterns of the $BiFeO_3$ materials.

The size-broadening of the reflections was used to estimate the crystallite size. The smallest crystallites are obtained at 803 K (BF1 : 46 nm). With increasing reaction temperature, the crystallite size increases up to 106 nm (BF3), and for BF4 the reflections are too narrow to detect size broadening. Specific BET surface areas may be used to calculate an effective particle diameter assuming cubic particle shape [43]. The surface areas of the materials are in a range from 6 to 61 m^2g^{-1} (Table 1, BF1–BF4). The calculated particle diameter shows the same trend, but the diameter is below the crystallite diameter calculated from the Scherrer equation. The latter could indicate the presence of pyrolytic carbon traces contributing to the specific surface area and thus the measured specific surface area is higher as compared to that expected from the ceramic nanoparticles alone. Insufficient removal of the matrix at 803 K is also evident from thermogravimetric studies showing a weight loss of 0.7% in between 803 K and 1103 K. However, both methods clearly reflect a particle size increasing with the synthesis temperature.

Scanning electron micrographs (Figure 2) reveal the granular shape of the particles with a broad particle size distribution and particle sizes varying from 30 to 90 nm for BF1. The particles are somewhat aggregated.

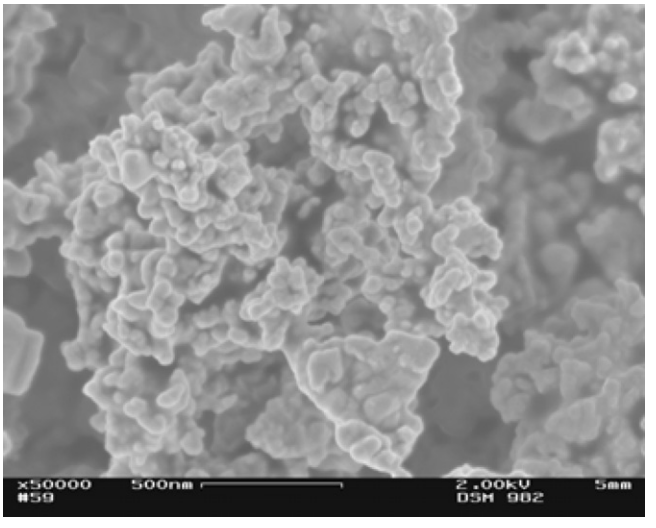

Figure 2. SEM image of $BiFeO_3$ nanoparticles (BF1).

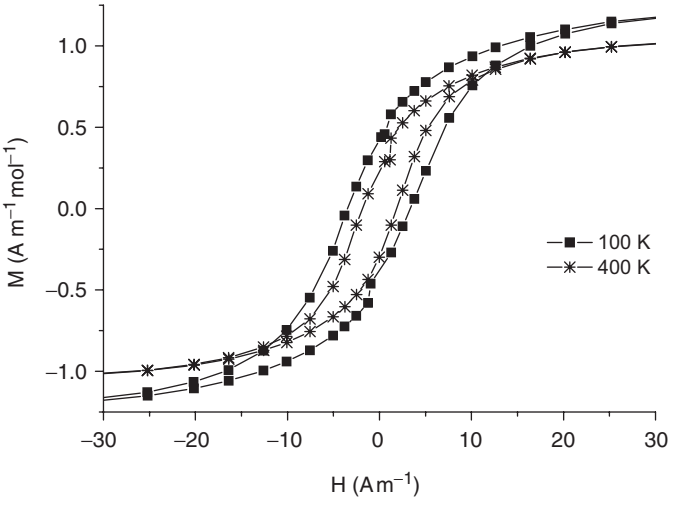

Figure 3. Field dependent magnetisation of $BiFeO_3$ nanoparticles (BF1).

The particles obtained from the matrix-assisted method are ferromagnetic and ferroelectric. The measured field-dependant magnetisation of the BF1 powder for temperatures at 100 K and 400 K are shown in Figure 3. As compared to the thin films prepared by a pulsed laser deposition technique onto single crystal $SrTiO_3(100)$ (STO) substrate reported by Wang et al. [12], the saturation magnetisation is $\sim 1.1\,A\,m^{-1}mol^{-1}$ and thus significantly lower as for 70-nm-thin $BiFeO_3$ films $5.6\,A\,m^{-1}mol^{-1}$. However, the coercive field is $1.88\,A\,m^{-1}$ at 400 K and $3.34\,A\,m^{-1}$ at 2 K and thus comparable to the values reported by Wang et al. with $2.51\,A\,m^{-1}$ at 400 K. The saturation magnetisation at

Table 2. Values for the coercive field and the saturation magnetisation in dependence of the applied temperature for the sample BF1.

T [K]	H_{coerce} [A m^{-1}]	M_{sat} [A m^{-1} mol^{-1}]
2	3.34	1.53
100	3.10	1.40
200	2.75	1.36
300	2.33	1.27
400	1.88	1.16

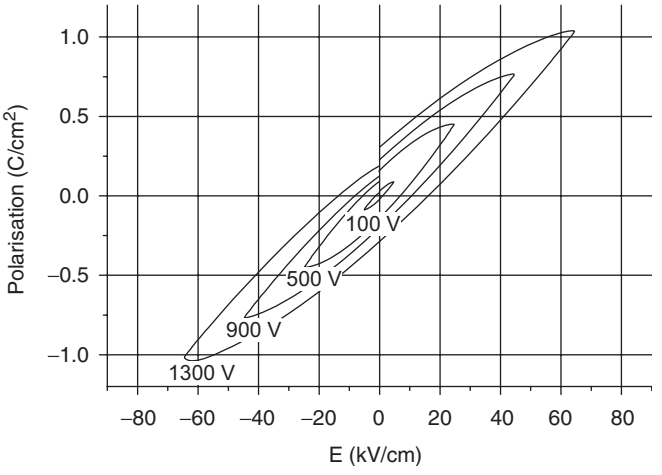

Figure 4. Hysteresis loops of $BiFeO_3$ nanoparticles (BF1).

252 A m^{-1} (not shown) of the particles decreases with increasing temperature from 1.53 A m^{-1} mol^{-1} (2 K) to 1.16 A m^{-1} mol^{-1} (400 K). The exact values for all measured temperatures are presented in Table 2. This slight decrease of the coercive field and the saturation magnetisation is characteristic for non-metallic, ferroelectric materials for a temperature range below the Curie temperature.

Ferroelectric hysteresis loops were measured using the Sawyer-Tower technique (Figure 4). Hysteresis loops were recorded, typical for unsaturated applied potentials. A low resistance has been reported earlier for $BiFeO_3$, rendering the measurement of ferroelectric loops sometimes difficult [42]. However, in BF1 synthesised at lower temperature, the conductivity was low and hysteresis measurements were carried out up to a certain potential which is below saturation. Above 1300 V the samples will be damaged by short cuts. Samples prepared at higher temperatures, like BF6, are of conductive nature and therefore not useable to perform ferroelectric hysteresis loops. A reason is probably the suppressed formation of Fe^{2+} allowing for measurements in between 100 and 1300 V [44]. A polarisation up to 1.04 μC/cm^2 was observed (E = 65 kV/cm) and the coercivity was 30.3 kV/cm. The latter is significantly lower as observed for thin films.

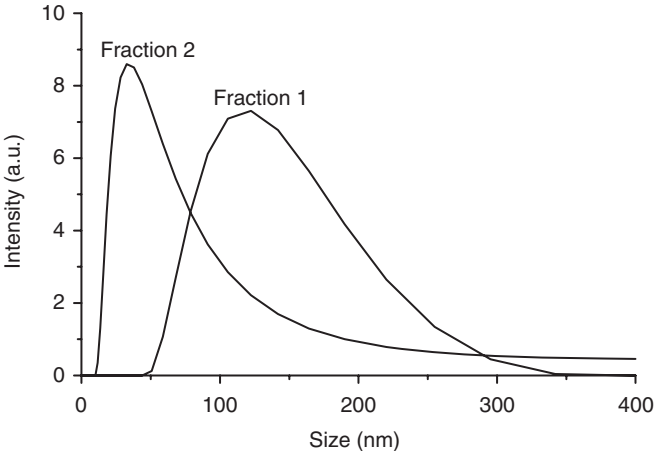

Figure 5. Particle size distribution of the $BiFeO_3$ nanoparticles in solution (THF).

3.2. *Dispersions of $BiFeO_3$ nanoparticles*

For the integration in polymers, the particles have to be further surface functionalised. Subsequent ball-milling with oleic acid, ultrasonification and centrifugation yield a clear and stable THF dispersion for BF1. This method was applied for the samples BF1–3. We found, that only the BF1 sample gave dispersions in a good yield. Above the preparation temperature for BF1, sintering effects cause irreversible aggregation. Consequently, this method is not a milling technique in the conventional sense. It is more a way to bring the stabiliser in contact with the particles.

With this method, approximately 50% of the BF1 powder can be dispersed. For all other samples no dispersions can be prepared. For the BF1/THF-dispersion, the excess of oleic acid can be removed using *n*-pentane for flocculation of the particles and THF for peptisation. Fractionation by centrifugation is achieved using different rotation rates (2000 and 6000 min^{-1}) resulting in a slightly turbid dispersion (fraction 1, 2000 min^{-1}) and dispersion with clear appearance (fraction 2, 6000 min^{-1}). The resulting two dispersions are characterised using dynamic light scattering (Figure 5). For fraction 1, a z-average of 114 nm, and for the fraction 2, a z-average of 30 nm was found (the z-average diameter is defined as the mean diameter based on the intensity weighed size distribution). While a $BiFeO_3$ content of 0.25 wt.% was observed for fraction 1 using thermal analysis, the solid content for fraction 2 was below 0.1%. Transmission electron micrographs confirm the presence of larger agglomerates in fraction 1 (Figure 6(a), with an inset of a single crystal of $BiFeO_3$ and its pseudo diffraction pattern proving the structural integrity of the dispersion containing nanoparticles) whereas in fraction 2 only particles in the range of 20 to 40 nm are detected (Figure 6(b)). Particles of the fraction 1 can be flocculated by adding *n*-pentane. Using XRD investigations the stability of the structure was identified and with it the multiferroic behaviour.

3.3. *Preparation of nanocomposites using $BiFeO_3$-dispersions*

Nanoparticulate, multiferroic $BiFeO_3$ within a transparent polymer could generate novel properties in the so formed nanocomposites. The incorporation in a polymer should in

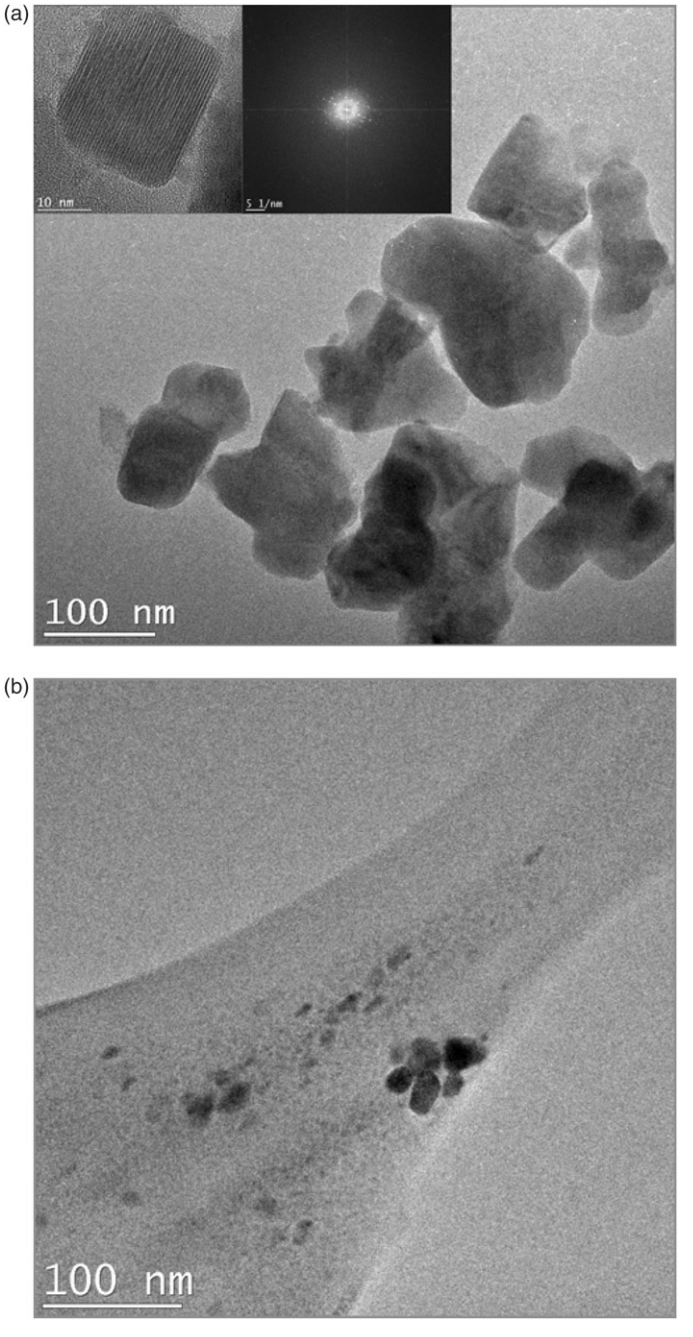

Figure 6. TEM images of the dried dispersion of $BiFeO_3$ in THF, (a) fraction 1 (inset: High Resolution Electron Microscopy (HRTEM) image and pseudo diffraction pattern from the Fourier transformation); (b) fraction 2.

principle result in a mulftiferroic nanocomposite, and the properties of performance polymers could be enhanced. To test the possibilities of embedding the nanoparticles into such matrices two typical representatives were chosen. PMMA as a relatively flexible and highly transparent isolating polymer and PVK as a stiff conductive polymer were the materials of choice. Not only the electric properties but also the processing of these polymers is quite different. The resulting glass temperatures of PMMA with $T \sim 374\,\mathrm{K}$ [45] and PVK with $T \sim 473\,\mathrm{K}$ [46] influence the processing and products as well.

4. Dip coating

Hybrid materials can be generated from a PMMA or a PVK containing dispersion of particles obtained from BF1 (fraction 1).

Dip coating can be applied to both the PMMA and PVK based composite films. Using the above mentioned mixtures it was possible to produce transparent films for $BiFeO_3$/PMMA and $BiFeO_3$/PVK. Here the evaporation of the solvent and the arrangement of the macromolecules in the case of PVK and PMMA result in transparent films. Different values of nanoparticle content can be achieved using this method. Figure 7(a) shows a dip coated film consisting of $BiFeO_3$ nanoparticles integrated inside a PVK matrix with a filler content of 11.9 wt% as the highest possible value and a transparency >90% in UV/Vis measurements. The particles are well integrated and only a small part of their surfaces can be identified using SEM.

5. Spin coating

Subsequent evaporation of the solvent by spin coating results in a thin film. Highly transparent films were obtained for the PMMA based composites, while experiments with PVK were not successful driven in order to achieve transparent films. Disintegration of these composites was characteristic for this method. A distribution of the particles with a low degree of aggregation is also detected in scanning electron micrographs.

Figure 7(b) shows the typical morphology of $BiFeO_3$/PMMA films obtained using spin coating with a filler content of only 0.5%. Here slight aggregation takes place, but a transparency of >90% is detected using UV/Vis measurements in the range of the visible light. The evaporation of the solvent during the spin coating process and the derived arrangement of the macromolecules is in the case of PVK too fast, and thus it is difficult to form a continuous composite film.

6. Evaporation/Pressing

Thicker films can be obtained from dry $BiFeO_3$/PMMA composites by pressing the polymer between two ITO-glasses at temperatures above the glass transition of the polymer. In Figure 8 the UV/Vis spectra of 40 μm thick films for three different $BiFeO_3$ concentrations (2.6, 5.4 and 7.6 wt.%) in PMMA, pure PMMA and $BiFeO_3$ dispersions are shown. As compared to pure PMMA, the transmittance is reduced in the visible range below 70% (600 nm). The transmittance decreases with increasing solid content as expected due to scattering in the red region whereas in the high energy range transmittance

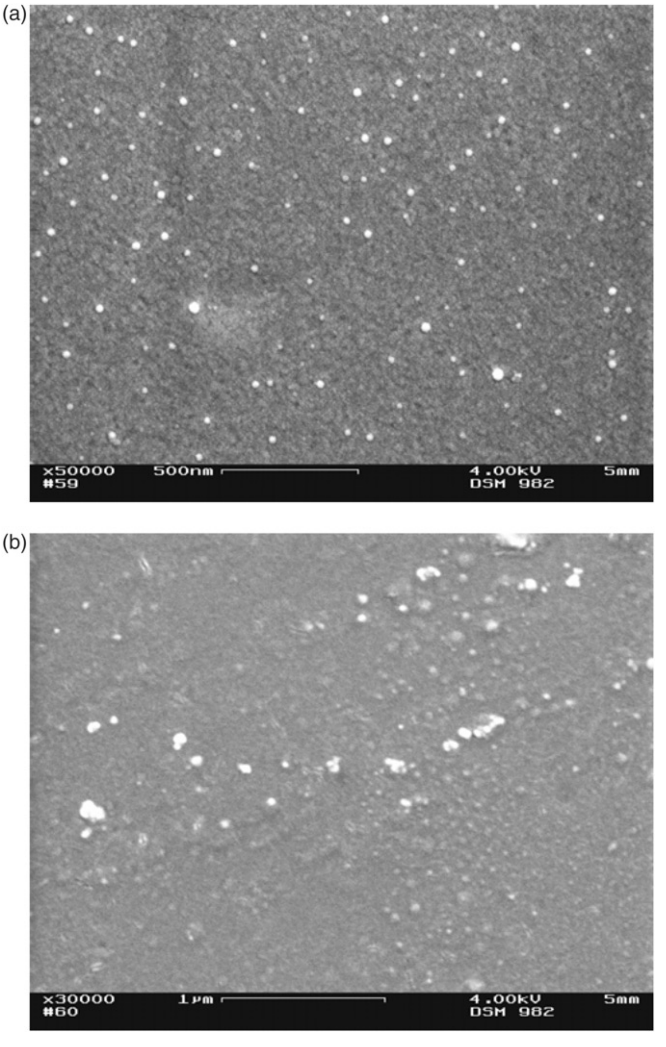

Figure 7. (a) $BiFeO_3$/PVK-film produced by dip coating technique; (b) $BiFeO_3$/PMMA-film produced by spin coating technique.

is also reduced due to light absorption by the particles. A strong absorption below 400 nm is also detected for diluted dispersions of the pure particles in THF.

Thick $BiFeO_3$/PVK composites could not be obtained. Phase separation and aggregation of the particles at these high temperatures but also decomposition of the composite containing components are responsible for this result. The PVK based composites always show disintegration and bubble formation.

7. Conclusions

$BiFeO_3$ nanoparticles were obtained using a carboneous matrix for sterical shielding suppressing sintering and crystal growth. Sufficient removal of the matrix and

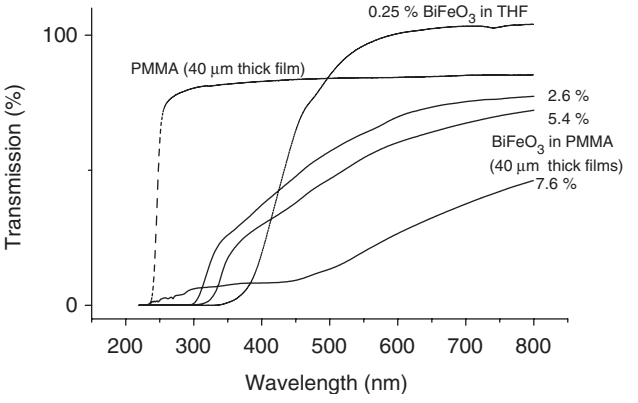

Figure 8. UV/Vis spectra of 40 μm thick films with different $BiFeO_3$ content and a 0.25 wt% $BiFeO_3$ solution in THF.

crystallisation of the particles was achieved at 803 K whereas higher temperatures result in decomposition of $BiFeO_3$ accompanied by the formation of impurities. The nanoparticles are ferromagnetic and ferroelectric. The highest saturation magnetisation was detected at 400 K with 1.16 A m^{-1} mol^{-1} and a coercive field of 1.88 A m^{-1}. Surface functionalisation allows the dispersion of $BiFeO_3$ nanoparticles in organic solvents. The integration of $BiFeO_3$ in transparent $BiFeO_3$/PMMA films was demonstrated successfully for spin and dip coating techniques, respectively for the evaporation/pressing process. The high T_g polymer PVK was only processed to form $BiFeO_3$/PVK composites using dip coating.

Acknowledgment

Financial support of the Federal Ministry of Education and Research (BMBF) is gratefully acknowledged (''Young Scientist Nanotechnology Initiative'', FK 03X5502).

References

[1] A. Vanrun, D.R. Terrell, and J.H. Scholing, *In situ grown eutectic magnetoelectric composite-material. 2. physical-properties*, J. Mater. Sci. 9 (1974), pp. 1710–1714.
[2] L.P.M. Bracke and R.G. Vanvliet, *A broad-band magnetoelectric transducer using a composite-material*, Int. J. Electron. 51 (1981), pp. 255–262.
[3] J. Ryu et al., *Piezoelectric and magnetoelectric properties of Lead Zirconate Titanate/Ni-Ferrite particulate composites*, J. Electroceram. 7 (2001), pp. 17–24.
[4] C.W. Nan et al., *Possible giant magnetoelectric effect of ferromagnetic rare-earth-iron-alloys-filled ferroelectric polymers*, Appl. Phys. Lett. 78 (2001), pp. 2527–2529.
[5] C.W. Nan, M. Li, and J.H. Huang, *Calculations of giant magnetoelectric effects in ferroic composites of rare-earth-iron alloys and ferroelectric polymers*, Phys. Rev. B 63(14) (2001), p. 144415.
[6] K. Mori and M. Wuttig, *Magnetoelectric coupling in terfenol-D/polyvinylidenedifluoride composites*, Appl. Phys. Lett. 81 (2002), pp. 100–101.

[7] N. Cai et al., *Dielectric, ferroelectric, magnetic, and magnetoelectric properties of multiferroic laminated composites*, Phys. Rev. B 68 (2003), p. 224103.
[8] M. Fiebig et al., *Observation of coupled magnetic and electric domains*, Nature 419 (2002), pp. 818–820.
[9] T. Lottermoser and M. Fiebig, *Magnetoelectric behavior of domain walls in multiferroic $HoMnO_3$*, Phys. Rev. B 70 (2004), p. 220407.
[10] N. Aliouane et al., *Field-induced linear magnetoelastic coupling in multiferroic $TbMnO_3$*, Phys. Rev. B 73 (2006), p. 020102.
[11] E. Golovenchits and V. Sanina, *Magnetic and magnetoelectric dynamics in RMn_2O_5 (R=Gd and Eu)*, J. Phys. Cond. Mater. 16 (2004), pp. 4325–4334.
[12] J. Wang et al., *Epitaxial $BiFeO_3$ multiferroic thin film heterostructures*, Science 299 (2003), pp. 1719–1722.
[13] A. Sharan et al., *Bismuth manganite: a multiferroic with a large nonlinear optical response*, Phys. Rev. B 69 (2004), p. 214109.
[14] S. Weber et al., *Colossal magnetocapacitance and colossal magnetoresistance in $HgCr_2S_4$*, Phys. Rev. Lett. 96 (2006), p. 157202.
[15] J. Hemberger et al., *Relaxor ferroelectricity and colossal magnetocapacitive coupling in ferromagnetic $CdCr_2S_4$*, Nature 434 (2005), pp. 364–367.
[16] H. Althues et al., *Integration of zinc oxide nanoparticles into transparent poly(butanediolmonoacrylate) via photopolymerisation*, J. Nanosci. Nanotechnol. 6 (2006), pp. 409–413.
[17] H. Althues et al., *Synthesis and characterization of transparent luminescent ZnS: Mn/PMMA nanocomposites*, Chem. Mater. 18 (2006), pp. 1068–1072.
[18] R. Palkovits et al., *Polymerization of w/o microemulsions for the preparation of transparent SiO_2/PMMA nanocomposites*, Langmuir 21 (2005), pp. 6048–6053.
[19] Q. Jiang, X.F. Cui, and M. Zhao, *Size effects on Curie temperature of ferroelectric particles*, Appl. Phys. A 78 (2004), pp. 703–704.
[20] T.J. Park, Y.B. Mao, and S.S. Wong, *Synthesis and characterization of multiferroic $BiFeO_3$ nanotubes*, Chem. Commun. (2004), pp. 2708–2709.
[21] Y.B. Mao, T.J. Park, and S.S. Wong, *Synthesis of classes of ternary metal oxide nanostructures*, Chem. Commun. (2005), pp. 5721–5735.
[22] S. Ghosh et al., *Low-temperature synthesis of nanosized bismuth ferrite by soft chemical route*, J. Am. Ceram. Soc. 88 (2005), pp. 1349–1352.
[23] S.P. Gubin, *Metalcontaining nano-particles within polymeric matrices: preparation, structure, and properties*, Colloids Surf. A 202 (2002), pp. 155–163.
[24] J.L. Wilson et al., *Synthesis and magnetic properties of polymer nanocomposites with embedded iron nanoparticles*, J. Appl. Phys. 95 (2004), pp. 1439–1443.
[25] E. Sowka et al., *Processing and properties of composite magnetic powders containing Co nanoparticles in polymer matrix*, J. Alloys Compd. 423 (2006), pp. 123–127.
[26] S.P. Gubin et al., *Magnetic and structural properties of Co nanoparticles in a polymer matrix*, J. Magn. Magn. Mater. 265 (2003), pp. 234–242.
[27] C. Baker, S.I. Shah, and S.K. Hasanain, *Magnetic behavior of iron and iron-oxide nanoparticle/polymer composites*, J. Magn. Magn. Mater. 280 (2004), pp. 412–418.
[28] D. Ciprari, K. Jacob, and R. Tannenbaum, *Characterization of polymer nanocomposite interphase and its impact on mechanical properties*, Macromolecules 39 (2006), pp. 6565–6573.
[29] T. Banert and U.A. Peuker, *Production of highly filled Fe_3O_4/PMMA nanocomposites by the spraying process*, Chem-Ing-Tech 77 (2005), pp. 224–227.
[30] H. Yang et al., *Preparation and optical constants of the nano-crystal and polymer composite $Bi_4Ti_3O_{12}$/PMMA thin films*, Opt. Laser Technol. 37 (2005), pp. 259–264.
[31] H. Yang et al., *Preparation and transmission loss of the nano-crystal and polymer composite film BTO/PMMA*, Opt. Laser Technol. 35 (2003), pp. 291–294.

[32] Q. Ren et al., *Refractive index dispersion on nano-crystal and polymer composite $Bi_4Ti_3O_{12}$/PEK-c films*, J. Mater. Sci. Lett. 21 (2002), pp. 677–678.
[33] B. Hilczer et al., *Dielectric relaxation in ferroelectric PZT-PVDF nanocomposites*, J. Non-Cryst. Solids 305 (2002), pp. 167–173.
[34] W.C. Liu et al., *Preparation and characterization of poled nanocrystal and polymer composite PZT/PC films*, Appl. Phys. A 81 (2005), pp. 543–547.
[35] Q. Ren et al., *Preparation and characterization of a poled nanocrystal and polymer composite $PbTiO_3$/PEK-c film for electro-optic applications*, Appl. Phys. A 76 (2003), pp. 183–186.
[36] D. Xu et al., *Study on the properties of a nanocrystal and polymer composite $PbTiO_3$/PEK-c film with optical anisotropy*, J. Mater. Sci. 39 (2004), pp. 6577–6582.
[37] F. Zhang et al., *Preparation of ferroelectric $(Pb,Sr)TiO_3$/polyethylene nanocomposites and their dielectric properties*, Jpn. J. Appl. Phys. 45 (2006), pp. 1873–1876.
[38] B. Hilczer et al., *Dielectric and pyroelectric response of $BaTiO_3$-PVDF nanocomposites*, Ferroelectrics 316 (2005), pp. 31–41.
[39] W.C. Liu et al., *Preparation and electro-optic properties of poled nanocrystals and polymer composite $BaTiO_3$/PC films*, Ferroelectrics 329 (2005), pp. 983–987.
[40] S. Brunauer, P.H. Emmett, and E. Teller, *Adsorption of gases in multimolecular layers*, J. Am. Chem. Soc. 60 (1938), pp. 309–319.
[41] P. Krawiec et al., *Oxide foams for the synthesis of high-surface-area vanadium nitride catalysts*, Adv. Mater. 18 (2006), pp. 505–508.
[42] Y.P. Wang et al., *Room-temperature saturated ferroelectric polarization in $BiFeO_3$ ceramics synthesized by rapid liquid phase sintering*, Appl. Phys. Lett. 84 (2004), pp. 1731–1733.
[43] F. Rouquerol, J. Rouquerol, and K. Sing, *Adsorption by powders & porous solids*, Academic Press, San Diego, 1998.
[44] A.K. Pradhan et al., *Magnetic and electrical properties of single-phase multiferroic $BiFeO_3$*, J. Appl. Phys. 97 (2005), p. 093903.
[45] K.G. Sturm, *Thermal dilation and glass transition as parameters for determining the viscosity of liquids*, Rheol. Acta 20 (1981), pp. 59–63.
[46] H. Bauser and W. Klopffer, *Excitons in polymers with aromatic side groups*, Kolloid Z. Z. Polym. 241 (1970), pp. 1026–1033.